

This item is the	he archived	peer-reviewed	author-	version c	of:

Optoelectronic properties of atomic layer deposited and sputtered MoS2 films

Reference:

Nattoo Crystal Alicia, Pena Tara, Nassiri Nazif Koosha, Wu Xiangjin, Rahimi Sepideh, D'Acunto Giulio, Bent Stacey F., Hadermann Joke, Pop Eric.-Optoelectronic properties of atomic layer deposited and sputtered MoS₂ films
ACS applied materials and interfaces - ISSN 1944-8252 - Washington, Amer chemical soc, 17:33(2025), p. 47347-47354
Full text (Publisher's DOI): https://doi.org/10.1021/ACSAMI.5C04483
To cite this reference: https://hdl.handle.net/10067/2159510151162165141

Optoelectronic properties of atomic layer deposited and sputtered MoS₂ Films

Crystal Alicia Nattoo^{1,†}, Tara Peña^{1,†}, Koosha Nassiri Nazif¹, Xiangjin Wu¹, Sepideh Rahimisheikh², Giulio D'Acunto³, Stacey Bent^{3,4}, Joke Hadermann², and Eric Pop^{1,4,5,a)}

ABSTRACT

Large-area growth techniques are needed to bring transition metal dichalcogenide (TMD) films into future applications, but some of these methods have not been sufficiently studied. Here, we evaluate and compare few-layer MoS₂ films (< 3 nm thick) grown by atomic layer deposition (ALD) and radio-frequency (RF) sputtering, using optical, topographical, X-ray spectroscopy, transmission electron microscopy, and electrical methods. The electron mobility of ALD films improves three-fold with a rapid thermal anneal, and these improvements are correlated with changes in their Raman spectra, such as a decrease of shoulder-to-E_{2g} peak ratio and a sharpening of the E_{2g} peak. On the other hand, the sputtered films had lower mobility and transistor current on/off ratio than the ALD samples, and the thermal anneal worsened both their surface roughness and electrical behavior. This work illustrates the utility of non-destructive materials characterization (e.g. Raman, with complementary techniques) to obtain a better picture of material quality before performing time-consuming device fabrication and electrical testing on emerging TMD films.

INTRODUCTION

Layered, atomically thin two-dimensional (2D) semiconductors have emerged in recent years with the promise of better charge mobility than conventional semiconductors at few-nanometer or sub-nanometer thickness. These materials can also be synthesized at sufficiently low temperatures as to be compatible with back-end-of-line (BEOL) or three-dimensional (3D) heterogeneous monolithic integration in conventional electronics, or even with more temperature-sensitive flexible substrates. Nevertheless, much research on 2D semiconductors, such as the transition metal dichalcogenides (TMDs), has relied on techniques such as mechanical exfoliation, which are not scalable to uniform, large-area films.

While chemical vapor deposition (CVD) has produced films for lab-scale experimentation, ¹⁰⁻¹⁴ the growth temperature often exceeds 500 °C, which is incompatible with heterogeneous 3D and flexible substrate integration. Instead – or in addition – techniques such as metal-organic CVD (MOCVD), ^{2, 15-19} atomic layer deposition (ALD), ²⁰⁻²⁵ and physical vapor deposition (sputtering)²⁶⁻³¹ provide other approaches that are also potentially more compatible with conventional, industrial semiconductor fabrication. Among these, ALD and sputtering have not been nearly as commonly studied as MOCVD, and more work is needed to understand their limitations and improve their quality. ^{22, 32-37}

In this study, we examine and compare the quality of few-layer (2-5 L) MoS₂ films prepared by ALD and radio-frequency (RF) sputtering, as-grown and with an annealing step hypothesized to improve film

¹Department of Electrical Engineering, Stanford University, Stanford, California 94305, USA

²Department of Physics, University of Antwerp, Antwerpen, Belgium

³Department of Chemical Engineering, Stanford University, Stanford, California 94305, USA

⁴Precourt Institute for Energy, Stanford University, Stanford, California 94305, USA

⁵Department of Materials Science and Engineering, Stanford University, Stanford, California 94305, USA

[†]These authors contributed equally to this work.

a) Author to whom correspondence should be addressed: epop@stanford.edu

quality. We analyze the films using Raman spectroscopy, X-ray photoelectron spectroscopy (XPS), transmission electron microscopy (TEM), atomic force microscopy (AFM), as well as electrical characterization – and uncover certain correlations between Raman or AFM features and the electrical behavior (i.e. transistor mobility and on/off current ratio) of the films. We expect that the metrology explored and the insights obtained in this work will aid in reducing future research and development timelines for implementing TMDs into electronic applications.

RESULTS AND DISCUSSION

i. Initial Material Study

The details of the MoS₂ ALD process have been described in previous work.³⁸ In brief, these films are prepared on 300 mm (12 inch) Si wafers covered by atomically flat thermal SiO₂, at a BEOL-compatible deposition temperatures of 500 °C [**Fig. 1(a)**]. Our RF sputtered MoS₂ films were prepared on similar substrates, but with lateral dimensions of a few centimeters [**Fig. 1(b)**], also at the same deposition temperature of 500 °C. Sputtering was done with 10 sccm Ar, 12 W RF power, and a pressure of 2 mTorr, from a bulk MoS₂ target of 2-inch diameter. The size of the target used and the deposition chamber size limit our sputtered film substrate size here, but this can be easily overcome in an industrial wafer-scale sputter process.

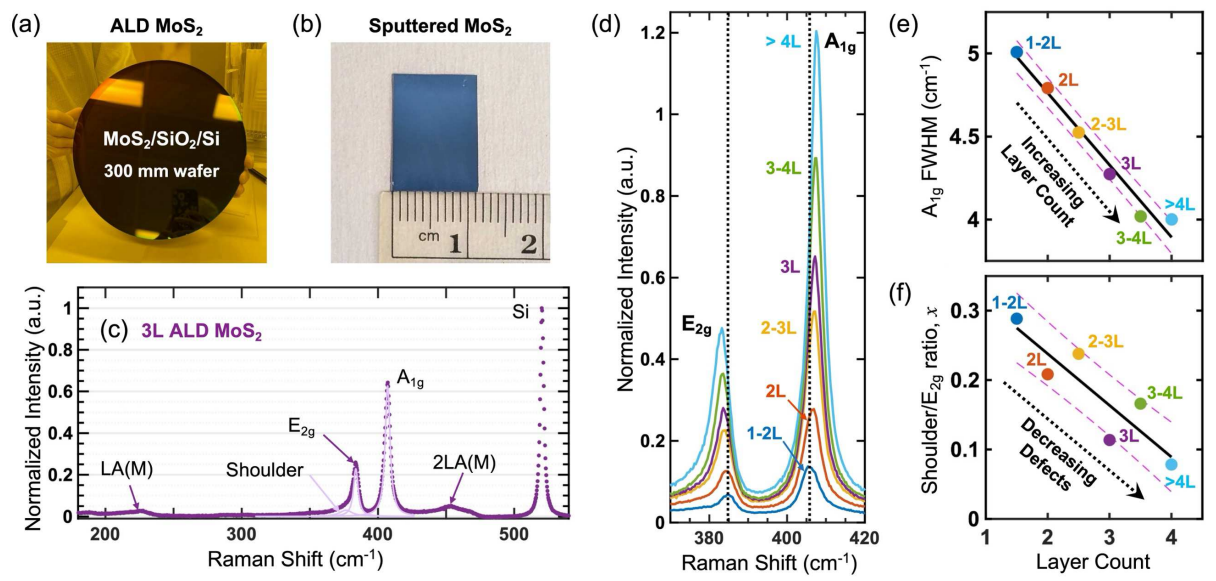


FIG. 1. (a) Photograph of 300 mm (12 inch) Si wafer covered by ALD MoS₂ on SiO₂/Si. **(b)** Photograph of SiO₂/Si substrates coated with RF sputtered MoS₂. **(c)** Measured Raman spectra on 3-layer (3L) ALD MoS₂ (symbols) with peak fittings (lines), normalized by the Si substrate peak at 520 cm⁻¹. **(d)** Raman spectra of ALD-grown films of various thicknesses, normalized by the Si substrate peak (not shown). Vertical dotted lines mark the E_{2g} and A_{1g} position expected of monolayer films. **(e)** Correlation between Raman A_{1g} peak full-width at half-maximum (FWHM) and thickness of ALD-grown MoS₂ films. **(f)** Correlation between Raman shoulder/E_{2g} intensity ratio (*x*) and thickness of ALD-grown MoS₂ films. Solid black lines are linear fits to the experimental data points. Pink dashed lines represent plus/minus one standard deviation (±1 STD) bounds of the fits.

To check and compare the optical quality of the films, we first employ Raman spectroscopy, which can directly and non-destructively probe defects, doping, and strain in MoS_2 . ^{39, 40} All Raman measurements were taken using a Horiba LabRAM instrument with a 100x short working distance objective, 532 nm excitation laser, 1800 l/mm grating, 150 μ m hole, and ~0.4 mW incident laser power. The laser power is

sufficiently low to avoid damage by heating of the MoS₂ films,⁴¹ but high enough for good signal-to-noise ratio. This setup enables a good resolution of 0.3 cm⁻¹ in each Raman spectrum [Fig. 1(c)]. The key Raman peaks were fit with a MATLAB script using a Voigt shape with a fixed Gaussian contribution to most accurately capture the line shape.⁴²⁻⁴⁴ The Gaussian component is due to instrument-related broadening, with a full-width at half-maximum (FWHM) of 1.31 cm⁻¹, estimated using the 277 cm⁻¹ peak from a neon lamp, and additional details about fitting are provided in Supporting Information Figs. S1 and S2. The Lorentzian FWHM of each spectrum, which corresponds to the sample's intrinsic FWHM, was then fit systematically over enough trials to converge to the lowest error between the fitted spectra and raw data.

The spectra for different layer thicknesses of ALD MoS₂ are shown in **Fig. 1(d)**. Thicker films have higher peak intensity, with red-shifting of the in-plane E_{2g} Raman mode and blue-shifting of the out-of-plane A_{1g} mode, as expected. The blue-shift of the A_{1g} mode from monolayer to bulk has been attributed to phonon stiffening with thickness, while the E_{2g} mode red-shift with thickness has been attributed to long range Columbic interactions. Higher than the FWHM of the A_{1g} peak decreases with increasing layer count, as summarized in **Fig. 1(e)**. Decreased FWHM for the first-order peaks is often used to indicate higher quality films, Higher than this metric is not sufficient, by itself. The improved film quality of the thicker films is also confirmed when plotting the shoulder-to- E_{2g} intensity ratio, x, in **Fig. 1(f)**. This estimates the MoS₂ sample quality by relying on defect-activated phonon modes which make up the "left shoulder" of the E_{2g} peak, with a lower ratio signifying lower defect density. Supporting Information **Fig. S3** plots a similar trend using the LA(M)/A_{1g} ratio, which is another way to estimate defectivity of MoS₂. From these results we conclude that the material quality is relatively improved for the thicker MoS₂ films due to the additional thermal annealing and time spent in the ALD chamber.

ii. Effect of Thermal Anneal on Material Quality

To investigate the effect of annealing as it relates to changing material quality and variability, several Raman maps were taken on both types of films (ALD and sputtered) as-grown and with an additional thermal anneal of 900 °C for 1 minute in an inert N_2 environment at 10 Torr pressure, in a rapid thermal processing chamber. The spectra were collected with a spot size of 0.5 μ m, in 5 μ m by 5 μ m maps with 1 μ m steps between each point, resulting in 25 spectra per measurement. Each sample was measured a minimum of two times to account for potential variability across the films.

Using the fitting approach described earlier, we extracted intensities and FWHMs for the three main features of interest: the E_{2g} shoulder, E_{2g} , and A_{1g} , as shown in **Fig. 2(a, b)**. **Figures 2(c, d)** summarize the evolution of the shoulder-to- E_{2g} ratio and the LA(M)-to- A_{1g} ratio for the as-grown ALD MoS₂ films and after the rapid thermal anneal. These films have an average shoulder-to- E_{2g} ratio of 0.325 ± 0.031 as-grown and 0.230 ± 0.068 after the anneal. This decrease in ratio suggests a lower defect density post-anneal, which matches well with other demonstrations of annealing in the literature. A similar trend is seen from the decrease in LA(M)-to- A_{1g} ratio in **Fig. 2(d)**, but we find the changes are more difficult to discern from the A_{1g} and E_{2g} FWHM [Supporting Information **Figs. S4(a)** and **S5(a)**].

Similarly, we analyze the RF-sputtered MoS₂ films as-grown and with the same thermal anneal. Relative to the Si substrate peak intensity (at 520 cm⁻¹), the sputtered film has lower intensity and broader FWHM for the A_{1g} peak [Fig. 3(a, b), as-grown and with anneal] compared to the ALD film [Fig. 2(a, b), as-grown and with anneal]. This is consistent with the higher-quality layers present in the ALD film, as we will see from high-resolution TEM analysis below. Overall, the sputtered MoS₂ films have lower quality both as-grown and annealed, than the ALD-grown films, as seen from all their Raman metrics. However,

the sputtered MoS₂ films display more obvious improvement with the thermal anneal, with Fig. 3(c) showing a decrease in the average shoulder-to- E_{2g} intensity ratio from 0.687 ± 0.022 to 0.507 ± 0.012 , as-grown and with annealing, respectively. The LA(M)-to- A_{1g} peak ratio [Fig. 3(d)] as well as the A_{1g} and E_{2g} FWHM of the sputtered MoS₂ film [Supporting Information Figs. S4(b) and S5(b)] similarly show more dramatic improvement with the anneal. This also indicates that the A_{1g} and E_{2g} FWHM are a reasonable gauge for higher-defectivity films (sputtered), but not for the lower-defectivity films (ALD).

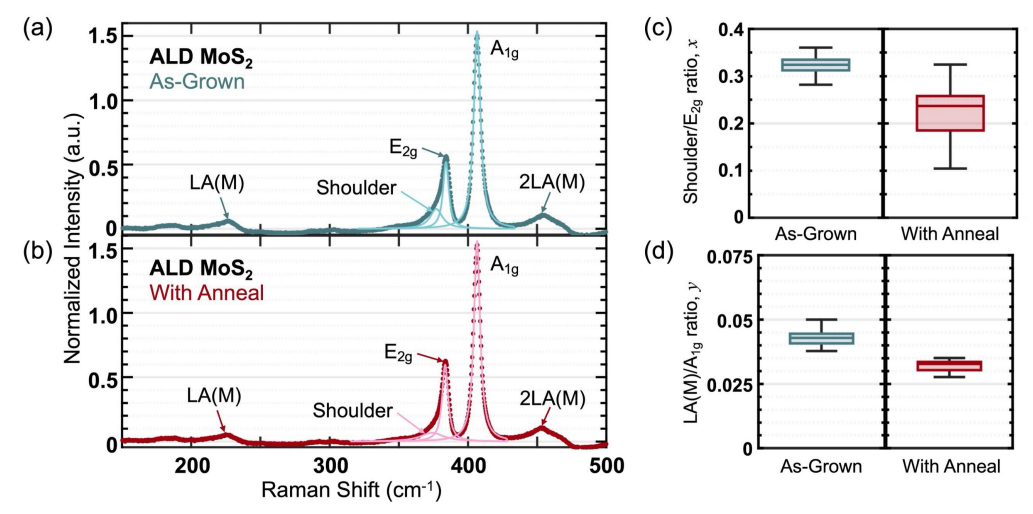


FIG. 2. Raman analysis of 3-4L thick ALD MoS₂ films. (a) As-deposited and (b) post-anneal, at 900 °C for 1 min. Symbols mark experimental data, lines are fits, after a linear background subtraction. (c) Ratio of shoulder-to- E_{2g} peak intensity, decreasing from 0.325 ± 0.031 (as-grown) to 0.230 ± 0.068 (after anneal). (d) Ratio of LA(M)-to-A_{1g} peak intensity, decreasing from 0.043 ± 0.003 (as-grown) to 0.032 ± 0.002 (after anneal). Each box plot represents 75 point spectra, taken over three regions of 5×5 points each, with 1 µm point spacing. All data were taken at room temperature and peak intensities are normalized to the Si peak.

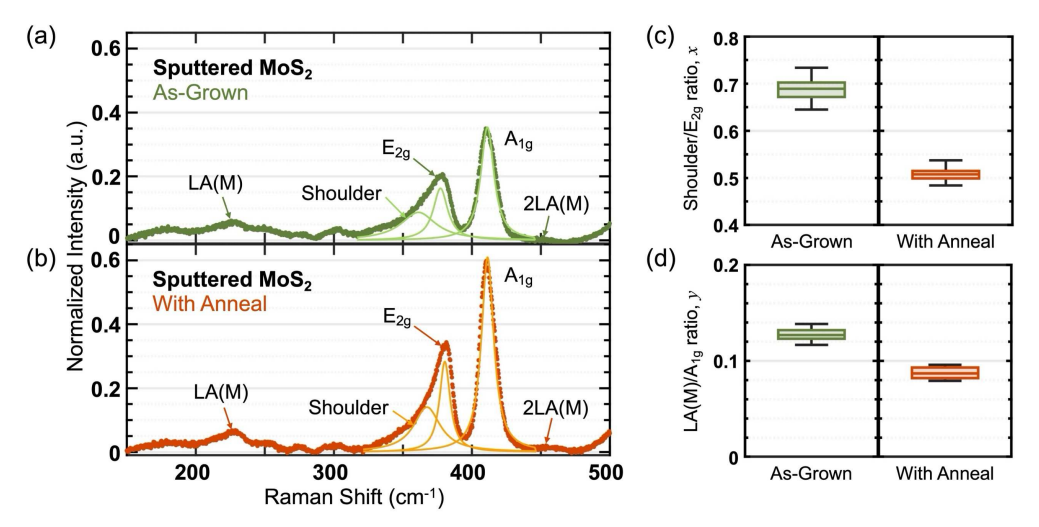


FIG. 3. Raman analysis of 3-4L thick RF-sputtered MoS₂ films. (a) As-deposited and (b) post-anneal, at 900 °C for 1 min. Symbols mark experimental data, lines are fits, after a linear background subtraction. (c) Ratio of shoulder-to- E_{2g} peak intensity, decreasing from 0.687 ± 0.022 (as-grown) to 0.507 ± 0.012 (annealed). (d) Ratio of LA(M)-to-A_{1g} peak intensity, decreasing from 0.128 ± 0.005 (as-grown) to 0.087 ± 0.007 (annealed). Each box plot represents 50 point spectra, taken over two regions of 5×5 points each, with 1 μm point spacing. All data were taken at room temperature and peak intensities are normalized to the Si peak.

To further investigate the nature of the two types of films, we carried out cross-sectional TEM with energy dispersive X-ray spectroscopy (EDX), as well as surface characterization by AFM, in Fig. 4. The sample cross-sections for TEM were prepared using a focused ion beam in scanning electron microscope (FIB-SEM) and capped with carbon-based epoxy prior to milling, as seen in Fig. 4(a, e). The ALD and RF-sputtered samples were separately imaged with probe-corrected Thermo Fisher Titan TEM microscopes at 200 and 300 kV, respectively. The ALD samples were imaged in high-resolution TEM (HRTEM) mode, while the sputtered samples were imaged in high-angle annular dark field scanning TEM (HAADF-STEM) mode. EDX analysis in Fig. 4(b, f) confirms the expected elemental composition. The ALD film cross-section in Fig. 4(a) shows a film thickness of ~2.1 nm, with 3 to 4 atomic layers of MoS₂. The sputtered film cross-section in Fig. 4(e) shows between 2 to 4 layers of MoS₂, from bright contrast Mo-Mo planes, and ~2.9 nm estimated film thickness.

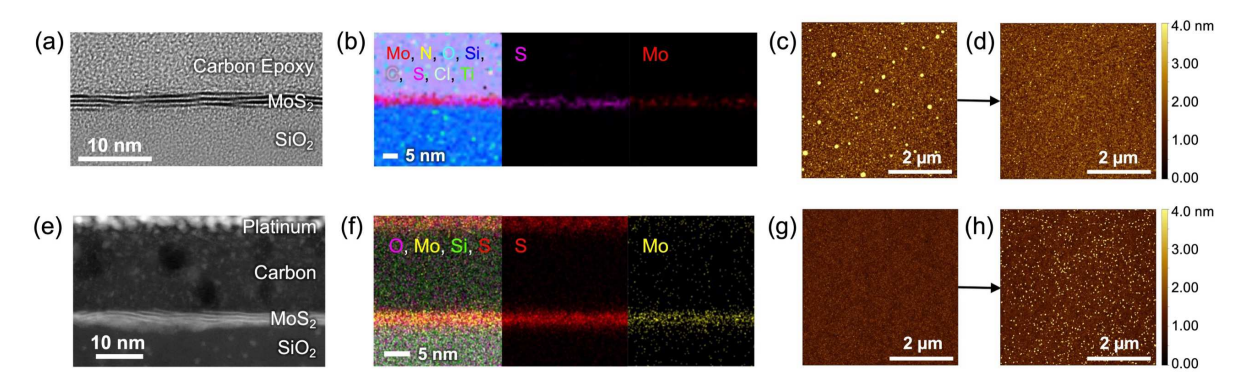


FIG. 4. (a) Cross-sectional TEM image and (b) TEM-EDX elemental analysis of the ALD MoS₂ film as-grown. (c) AFM surface roughness scan of ALD MoS₂ film as-grown and (d) with anneal, showing decreased surface roughness. (e) Cross-sectional STEM image and (f) TEM-EDX elemental analysis of the RF-sputtered MoS₂ film as-grown. (g) AFM scan of RF sputtered MoS₂ film as-grown and (h) with anneal, showing increased surface roughness.

Interestingly, we observed that the rapid thermal anneal step had different effects on the surface roughness of ALD vs. sputtered MoS₂ films. We image the topographical changes using a Bruker Icon AFM, with a NSC18/Pt tip in tapping mode. The surface of the ALD films as-grown [Fig. 4(c)] displays several large regions over 4 nm tall, but with the anneal [Fig. 4(d)] these regions largely disappear, resulting in a more uniform film, consistent with the result of similar anneals in the literature.⁴⁸ The sputtered films tell a different story. Fig. 4(g) shows that the sputtered MoS₂ films start out more uniform and flatter, with a root-mean-square (rms) surface roughness of 276.8 pm. With annealing, the rms surface roughness increases to 759.4 pm [Fig. 4(h)], due to the appearance of small speckles scattered across the film. XPS measurements, provided in Supporting Information Fig. S6, suggest the overall stoichiometry remains relatively unchanged as-grown and with anneal, minimizing the possibility of oxidation being the culprit. However, previous studies^{49, 50} have suggested that such vertical domains can be produced, resulting in a film that was discontinuous laterally. Vertical domains are postulated to derive from MoS₂ islands, which evolve into vertical domains owing to competing defect and strain energies.^{50, 51}

To evaluate the electrical characteristics of these films, we fabricated back-gated field-effect transistors (FETs), with schematic displayed in **Fig. 5(a)**. The 3-4 layer MoS₂ films were directly deposited (by ALD or sputtering) onto 96 nm SiO₂ on p⁺⁺ Si, which also serves as a back-gate. The films used for electrical characterization are from the same deposition process as those used for TEM measurements. All device lithography steps were carried out on a Raith EBPG 5200+, forming 2 µm wide channels, patterned with

XeF₂ etch, and source/drain contacts consisting of 50 nm thick Au, without an adhesion layer.¹ Devices were made as part of transfer length method (TLM) structures⁵² with varying channel lengths from 0.1 μm to 1 μm. The devices are placed in a vacuum probe station ($\sim 10^{-5}$ torr) and annealed at 250 °C for 2 hours, to remove adsorbates from the channel and to improve the contacts. We measured the drain current I_D vs. back-gate voltage V_{GS} , at $V_{DS} = 0.1$ V, without breaking vacuum and after the samples cooled down to room temperature, as illustrated in **Figs. 5(b-d)**. Using TLM analysis, we estimated the effective MoS₂ channel mobility from the slope of the total device resistance (at a fixed overdrive voltage¹) vs. channel length, as shown in Supporting Information **Fig. S7**.

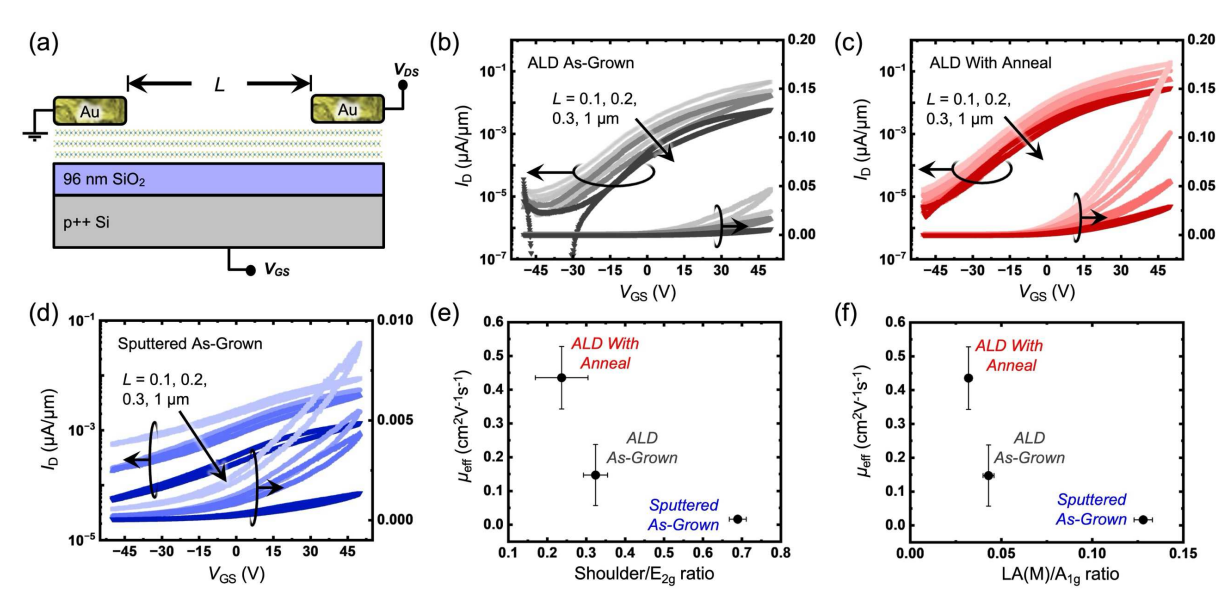


FIG. 5. (a) Cross-sectional schematic of back-gated transistors used to estimate electron mobility in our ALD and sputtered MoS₂ films. **(b)** Measured transfer characteristics (I_D vs. V_{GS}) of ALD MoS₂ as-grown and **(c)** with anneal. **(d)** Measured I_D vs. V_{GS} of RF sputtered MoS₂ transistors as-grown. For (b-d), the data are shown on log (left) and linear (right) axes, from four channel lengths, as labeled; forward and backward V_{GS} sweeps reveal some clockwise hysteresis and all transfer characteristics are with $V_{DS} = 0.1$ V. **(e)** Relationship between estimated MoS₂ mobility and Raman shoulder-to-E_{2g} intensity ratio across 5 devices for each film. Error bars represent standard deviations across the measured data. **(f)** Relationship between estimated MoS₂ mobility and Raman LA(M)-to-A_{1g} intensity ratio across all measured devices. Sputtered film data with anneal are not shown, as they were all open-circuit.

For the shortest ALD MoS₂ devices, we observe a nearly 4× increase in maximum current density with the anneal step, as shown in **Fig. 5(b, c)**. Moreover, the current ratio $I_{\rm on}/I_{\rm off}$ increases by an order of magnitude, from ~10³ to ~10⁴. The hysteresis also improves and, together, these observations suggest a reduction of the number of defects and traps in the ALD films with the anneal step. On the other hand, the sputtered films display an order of magnitude lower current and effective mobility (than the ALD films) as-grown [**Fig. 5(d, e)**], and their modest $I_{\rm on}/I_{\rm off}$ ratio is comparable to previous reports for sputtered MoS₂ films of similar thickness⁵³. However, all sputtered MoS₂ films appeared to be open-circuit with the thermal anneal, and this degradation occurred likely due to vertical domain production⁵⁰ and resulting discontinuity of MoS₂ film revealed in the AFM surface analysis, in **Fig. 4(h)**. The effective mobility from TLM measurements of these films is summarized in **Fig. 5(e, f)**. The mobility was estimated to be 0.44 ± 0.09 cm²V⁻¹s⁻¹ at room temperature in the ALD MoS₂ films with the anneal step, and the mobility (in general) is observed to scale inversely with the shoulder-to-E_{2g} and the LA(M)-to-A_{1g} intensity ratios, as expected.

CONCLUSIONS

We have evaluated and compared few-layer MoS_2 films produced by two large-area synthesis methods (atomic layer deposition and sputtering) by optical, topographical, X-ray, transmission electron microscopy, and electrical measurements. The ALD films, in general, have better Raman features (e.g. lower shoulder-to- E_{2g} and LA(M)-to- A_{1g} intensity ratios, as well as lower E_{2g} and A_{1g} FWHMs), higher transistor current on/off ratio, as well as higher mobility, and these metrics improve with a rapid thermal anneal. In contrast, the sputtered films have higher surface roughness with the anneal, and their electrical behavior degrades. This does not necessarily mean that one must always choose ALD over sputtered films, but the present study does provide a snapshot of these recent results, which are important for future improvements in both types of films. In particular, the observed correlation between Raman features and the electrical quality of the films suggests that such optical measurements can be used to rapidly screen the quality of 2D material layers in the future, while their synthesis is optimized, without having to rely on more time-consuming device fabrication and electrical measurements. Besides improving the synthesis process, future work must also investigate different industry-compatible anneal conditions that improve film quality and reduce defects which may inadvertently form during synthesis.

ACKNOWLEDGMENTS

The authors thank Christina Newcomb for assistance with neon lamp spectral width calibration for Raman analysis and EMD Electronics for assistance with TEM on the ALD film. Part of this work was performed at the Stanford Nano Shared Facilities (SNSF), supported by the National Science Foundation (NSF) under award ECCS-2026822. C.A.N. acknowledges support from the NSF Graduate Fellowship Program. T.P. acknowledges support from the NSF MPS-Ascend Postdoctoral Fellowship. G.D. acknowledges support from Wallenberg Foundation Postdoctoral Scholarship Program KAW 2021.0342. C.A.N., K.N.N., and E.P. also acknowledge support from the Department of Energy Grant DE-AC02-06CH11357. X.W., T.P., and E.P. acknowledge partial support from PRISM and SUPREME, JUMP 2.0 Centers sponsored by the Semiconductor Research Corporation (SRC) and DARPA.

REFERENCES

- (1) English, C. D.; Shine, G.; Dorgan, V. E.; Saraswat, K. C.; Pop, E. Improved Contacts to MoS₂ Transistors by Ultra-High Vacuum Metal Deposition. *Nano Lett.* **2016**, *16* (6), 3824-3830.
- (2) Chowdhury, S.; Roy, A.; Liu, C.; Alam, M. H.; Ghosh, R.; Chou, H.; Akinwande, D.; Banerjee, S. K. Two-Step Growth of Uniform Monolayer MoS₂ Nanosheets by Metal-Organic Chemical Vapor Deposition. *ACS Omega* **2021**, *6* (15), 10343-10351.
- (3) Park, J. H.; Lu, A. Y.; Shen, P. C.; Shin, B. G.; Wang, H.; Mao, N.; Xu, R.; Jung, S. J.; Ham, D.; Kern, K.; et al. Synthesis of High-Performance Monolayer Molybdenum Disulfide at Low Temperature. *Small Methods* **2021**, *5* (6), 2000720.
- (4) Park, Y. J.; Sharma, B. K.; Shinde, S. M.; Kim, M. S.; Jang, B.; Kim, J. H.; Ahn, J. H. All MoS₂-Based Large Area, Skin-Attachable Active-Matrix Tactile Sensor. *ACS Nano* **2019**, *13* (3), 3023-3030.
- (5) Li, N.; Wang, Q. Q.; Shen, C.; Wei, Z.; Yu, H.; Zhao, J.; Lu, X. B.; Wang, G. L.; He, C. L.; Xie, L.; et al. Large-scale flexible and transparent electronics based on monolayer molybdenum disulfide field-effect transistors. *Nat. Electron.* **2020**, *3* (11), 711-717.
- (6) Daus, A.; Vaziri, S.; Chen, V.; Köroglu, C.; Grady, R. W.; Bailey, C. S.; Lee, H. R.; Schauble, K.; Brenner, K.; Pop, E. High-performance flexible nanoscale transistors based on transition metal dichalcogenides. *Nat. Electron.* **2021**, *4* (7), 495-501.
- (7) Shinde, S. M.; Das, T.; Hoang, A. T.; Sharma, B. K.; Chen, X.; Ahn, J. H. Surface-Functionalization-Mediated Direct Transfer of Molybdenum Disulfide for Large-Area Flexible Devices. *Adv. Funct. Mater.* **2018**, *28*, 1706231.

- (8) Hoang, A. T.; Hu, L.; Katiyar, A. K.; Ahn, J.-H. Two-dimensional layered materials and heterostructures for flexible electronics. *Matter* **2022**, *5* (12), 4116-4132.
- (9) Hoang, A. T.; Hu, L.; Kim, B. J.; Van, T. T. N.; Park, K. D.; Jeong, Y.; Lee, K.; Ji, S.; Hong, J.; Katiyar, A. K.; et al. Low-temperature growth of MoS₂ on polymer and thin glass substrates for flexible electronics. *Nat. Nanotechnol.* **2023**, *18* (12), 1439-1447.
- (10) Smithe, K. K. H.; Suryavanshi, S. V.; Munoz Rojo, M.; Tedjarati, A. D.; Pop, E. Low Variability in Synthetic Monolayer MoS₂ Devices. *ACS Nano* **2017**, *11* (8), 8456-8463.
- (11) Smithe, K. K. H.; English, C. D.; Suryavanshi, S. V.; Pop, E. Intrinsic electrical transport and performance projections of synthetic monolayer MoS₂ devices. 2D Mater. 2017, 4 (1), 011009
- (12) Wu, X. Y.; Lin, D.; Cott, D.; De Marneffe, J. F.; Groven, B.; Sergeant, S.; Shi, Y. Y.; Smets, Q.; Sutar, S.; Asselberghs, I.; et al. ALD Encapsulation of CVD WS₂ for Stable and High-Performance FET Devices. In 2021 Electron Devices Technology and Manufacturing Conference (EDTM), 2021.
- (13) Zhang, Y.; Yao, Y.; Sendeku, M. G.; Yin, L.; Zhan, X.; Wang, F.; Wang, Z.; He, J. Recent Progress in CVD Growth of 2D Transition Metal Dichalcogenides and Related Heterostructures. *Adv. Mater.* **2019**, *31* (41), 1901694.
- (14) Sousa, F. B.; Nadas, R.; Martins, R.; Barboza, A. P. M.; Soares, J. S.; Neves, B. R. A.; Silvestre, I.; Jorio, A.; Malard, L. M. Disentangling doping and strain effects at defects of grown MoS₂ monolayers with nano-optical spectroscopy. *Nanoscale* **2024**, *16* (27), 12923-12933.
- (15) Cwik, S.; Mitoraj, D.; Reyes, O. M.; Rogalla, D.; Peeters, D.; Kim, J.; Schütz, H. M.; Bock, C.; Beranek, R.; Devi, A. Direct Growth of MoS₂ and WS₂ Layers by Metal Organic Chemical Vapor Deposition. *Adv. Mater. Interfaces* **2018**, *5* (16), 1800140.
- (16) Cohen, A.; Patsha, A.; Mohapatra, P. K.; Kazes, M.; Ranganathan, K.; Houben, L.; Oron, D.; Ismach, A. Growth-Etch Metal-Organic Chemical Vapor Deposition Approach of WS₂ Atomic Layers. *ACS Nano* **2021**, *15* (1), 526-538.
- (17) Mun, J.; Park, H.; Park, J.; Joung, D.; Lee, S. K.; Leem, J.; Myoung, J. M.; Park, J.; Jeong, S. H.; Chegal, W. C.; et al. High-Mobility MoS₂ Directly Grown on Polymer Substrate with Kinetics-Controlled Metal-Organic Chemical Vapor Deposition. *ACS Appl. Electron. Mater.* **2019**, *1* (4), 608-616.
- (18) Wang, Z.; Tripathi, M.; Golsanamlou, Z.; Kumari, P.; Lovarelli, G.; Mazziotti, F.; Logoteta, D.; Fiori, G.; Sementa, L.; Marega, G. M.; et al. Substitutional p-Type Doping in NbS₂ -MoS₂ Lateral Heterostructures Grown by MOCVD. *Adv. Mater.* **2023**, *35* (14), 2209371.
- (19) Gong, Y. Y.; Zhang, X. T.; Redwing, J. M.; Jackson, T. N. Thin Film Transistors Using Wafer-Scale Low-Temperature MOCVD WSe₂. *J. Electron. Mater.* **2016**, *45* (12), 6280-6284.
- (20) Zhang, T.; Wang, Y.; Xu, J.; Chen, L.; Zhu, H.; Sun, Q.; Ding, S.; Zhang, D. W. High performance few-layer MoS₂ transistor arrays with wafer level homogeneity integrated by atomic layer deposition. *2D Mater.* **2017**, *5* (1), 015028.
- (21) Shi, M. L.; Chen, L.; Zhang, T. B.; Xu, J.; Zhu, H.; Sun, Q. Q.; Zhang, D. W. Top-Down Integration of Molybdenum Disulfide Transistors with Wafer-Scale Uniformity and Layer Controllability. *Small* **2017**, *13* (35), 1603157.
- (22) Tian, Z. L.; Zhao, D. H.; Liu, H.; Zhu, H.; Chen, L.; Sun, Q. Q.; Zhang, D. W. Optimization of Defects in Large-Area Synthetic MoS₂ Thin Films by CS₂ Treatment for Switching and Sensing Devices. *ACS Appl. Nano Mater.* **2019**, *2* (12), 7810-7818.
- (23) Liu, H.; Chen, L.; Zhu, H.; Sun, Q. Q.; Ding, S. J.; Zhou, P.; Zhang, D. W. Atomic layer deposited 2D MoS₂ atomic crystals: from material to circuit. *Nano Res.* **2020**, *13* (6), 1644-1650.
- (24) Aspiotis, N.; Morgan, K.; März, B.; Müller-Caspary, K.; Ebert, M.; Weatherby, E.; Light, M. E.; Huang, C. C.; Hewak, D. W.; Majumdar, S.; et al. Large-area synthesis of high electrical performance MoS₂ by a commercially scalable atomic layer deposition process. *npj 2D Mater. Appl.* **2023**, *7* (1), 18.
- (25) Jeon, W.; Cho, Y.; Jo, S.; Ahn, J. H.; Jeong, S. J. Wafer-Scale Synthesis of Reliable High-Mobility Molybdenum Disulfide Thin Films via Inhibitor-Utilizing Atomic Layer Deposition. *Adv. Mater.* **2017**, *29* (47).
- (26) Kitazawa, T.; Inaba, Y.; Yamashita, S.; Imai, S.; Kurohara, K.; Tatsumi, T.; Wakabayashi, H.; Tomiya, S. Impact of crystallinity on thermal conductivity of RF magnetron sputtered MoS₂ thin films. *Jpn. J. Appl. Phys.* **2024**, *63* (5), 055508
- (27) Wahid, S.; Daus, A.; Khan, A. I.; Chen, V.; Neilson, K. M.; Islam, M.; Chen, M. E.; Pop, E. Lateral electrical transport and field-effect characteristics of sputtered p-type chalcogenide thin films. *Appl. Phys. Lett.* **2021**, *119* (23), 232106.
- (28) Gupta, D.; Chauhan, V.; Kumar, R. Sputter deposition of 2D MoS₂ thin films A critical review from a surface and structural perspective. *Inorg. Chem. Commun.* **2022**, *144*, 109848.

- (29) Park, H.; Liu, N.; Kim, B. H.; Kwon, S. H.; Baek, S.; Kim, S.; Lee, H. K.; Yoon, Y. J.; Kim, S. Exceptionally Uniform and Scalable Multilayer MoS₂ Phototransistor Array Based on Large-Scale MoS₂ Grown by RF Sputtering, Electron Beam Irradiation, and Sulfurization. *ACS Appl. Mater. Interfaces* **2020**, *12* (18), 20645-20652.
- (30) Choudhary, N.; Park, J.; Hwang, J. Y.; Choi, W. Growth of large-scale and thickness-modulated MoS₂ nanosheets. *ACS Appl. Mater. Interfaces* **2014**, *6* (23), 21215-21222.
- (31) Huang, J. H.; Chen, H. H.; Liu, P. S.; Lu, L. S.; Wu, C. T.; Chou, C. T.; Lee, Y. J.; Li, L. J.; Chang, W. H.; Hou, T. H. Large-area few-layer MoS₂ deposited by sputtering. *Mater. Res. Express* **2016**, *3* (6), 065007.
- (32) Edelberg, D.; Rhodes, D.; Kerelsky, A.; Kim, B.; Wang, J.; Zangiabadi, A.; Kim, C.; Abhinandan, A.; Ardelean, J.; Scully, M.; et al. Approaching the Intrinsic Limit in Transition Metal Diselenides via Point Defect Control. *Nano Lett.* **2019**, *19* (7), 4371-4379.
- (33) Tian, X.; Yan, X.; Varnavides, G.; Yuan, Y.; Kim, D. S.; Ciccarino, C. J.; Anikeeva, P.; Li, M. Y.; Li, L. J.; Narang, P.; et al. Capturing 3D atomic defects and phonon localization at the 2D heterostructure interface. *Sci. Adv.* **2021**, *7* (38), eabi6699.
- (34) Wu, Z. T.; Luo, Z. Z.; Shen, Y. T.; Zhao, W. W.; Wang, W. H.; Nan, H. Y.; Guo, X. T.; Sun, L. T.; Wang, X. R.; You, Y. M.; et al. Defects as a factor limiting carrier mobility in WSe₂: A spectroscopic investigation. *Nano Res.* **2016**, *9* (12), 3622-3631.
- (35) Zhang, X.; Xu, J.; Zhi, A.; Wang, J.; Wang, Y.; Zhu, W.; Han, X.; Tian, X.; Bai, X.; Sun, B.; et al. Low-Defect-Density Monolayer MoS₂ Wafer by Oxygen-Assisted Growth-Repair Strategy. *Adv. Sci.* **2024**, *11* (42), 2408640.
- (36) Xiao, Z.; Guo, R.; Zhang, C.; Liu, Y. Point Defect Limited Carrier Mobility in 2D Transition Metal Dichalcogenides. *ACS Nano* **2024**, *18* (11), 8511-8516.
- (37) Fang, L.; Chen, H.; Yuan, X.; Huang, H.; Chen, G.; Li, L.; Ding, J.; He, J.; Tao, S. Quick Optical Identification of the Defect Formation in Monolayer WSe₂ for Growth Optimization. *Nanoscale Res. Lett.* **2019**, *14* (1), 274.
- (38) Ngo, T.; Zacatzi, A.; Tan, Y.; Lee, D.; Waknis, A.; Vu, N.; Kanjolia, R.; Moinpour, M.; Chen, Z. 300mm Waferscale ALD-grown MoS₂ for Cu diffusion barrier. In 2024 IEEE International Interconnect Technology Conference (IITC), 2024.
- (39) Mignuzzi, S.; Pollard, A. J.; Bonini, N.; Brennan, B.; Gilmore, I. S.; Pimenta, M. A.; Richards, D.; Roy, D. Effect of disorder on Raman scattering of single-layer MoS₂. *Phys. Rev. B: Condens. Matter* **2015**, *91* (19), 195411. (40) Shi, W.; Zhang, X.; Li, X.-L.; Qiao, X.-F.; Wu, J.-B.; Zhang, J.; Tan, P.-H. Phonon Confinement Effect in Two-
- dimensional Nanocrystallites of Monolayer MoS₂ to Probe Phonon Dispersion Trends Away from Brillouin-Zone Center. *Chin. Phys. Lett.* **2016**, *33* (5), 057801.
- (41) Yalon, E.; Aslan, B.; Smithe, K. K. H.; McClellan, C. J.; Suryavanshi, S. V.; Xiong, F.; Sood, A.; Neumann, C. M.; Xu, X.; Goodson, K. E.; et al. Temperature-Dependent Thermal Boundary Conductance of Monolayer MoS₂ by Raman Thermometry. *ACS Appl. Mater. Interfaces* **2017**, *9* (49), 43013-43020.
- (42) Zaghloul, M. R. On the calculation of the Voigt line profile: a single proper integral with a damped sine integrand. *Monthly Notices of the Royal Astronomical Society* **2007**, *375* (3), 1043-1048.
- (43) Michail, A.; Delikoukos, N.; Parthenios, J.; Galiotis, C.; Papagelis, K. Optical detection of strain and doping inhomogeneities in single layer MoS₂. *Appl. Phys. Lett.* **2016**, *108* (17), 173102.
- (44) Ulrich, C.; Anastassakis, E.; Syassen, K.; Debernardi, A.; Cardona, M. Lifetime of Phonons in Semiconductors under Pressure. *Phys. Rev. Lett.* **1997**, *78* (7), 1283-1286.
- (45) Lee, C.; Yan, H.; Brus, L. E.; Heinz, T. F.; Hone, J.; Ryu, S. Anomalous lattice vibrations of single- and few-layer MoS₂. ACS Nano **2010**, 4 (5), 2695-2700.
- (46) Zhang, X.; Qiao, X. F.; Shi, W.; Wu, J. B.; Jiang, D. S.; Tan, P. H. Phonon and Raman scattering of two-dimensional transition metal dichalcogenides from monolayer, multilayer to bulk material. *Chem. Soc. Rev.* **2015**, *44* (9), 2757-2785.
- (47) Dash, A. K.; Swaminathan, H.; Berger, E.; Mondal, M.; Lehenkari, T.; Prasad, P. R.; Watanabe, K.; Taniguchi, T.; Komsa, H.-P.; Singh, A. Evidence of defect formation in monolayer MoS₂ at ultralow accelerating voltage electron irradiation. *2D Mater.* **2023**, *10* (3), 035002.
- (48) Wen, M.; Xu, J.; Liu, L.; Lai, P.-T.; Tang, W.-M. Improved Electrical Performance of Multilayer MoS₂ Transistor With NH₃-Annealed ALD HfTiO Gate Dielectric. *IEEE Trans. Electron Devices* **2017**, *64* (3), 1020-1025. (49) Chen, G.; Lu, B.; Cui, X.; Xiao, J. Effects of Deposition and Annealing Temperature on the Structure and
- Optical Band Gap of MoS₂ Films. *Materials* **2020**, *13* (23), 5515.
- (50) Wadhwa, R.; Thapa, S.; Deswal, S.; Kumar, P.; Kumar, M. Wafer-scale controlled growth of MoS₂ by magnetron sputtering: from in-plane to inter-connected vertically-aligned flakes. *J. Phys.: Condens. Matter* **2023**, *35* (12), 124002.
- (51) Li, H.; Wu, H.; Yuan, S.; Qian, H. Synthesis and characterization of vertically standing MoS₂ nanosheets. *Sci. Rep.* **2016**, *6*, 21171.

(52) Schroder, D. K. Semiconductor Material and Device Characterization; Wiley, 2015.

(53) Matsuura, K.; Hamada, M.; Hamada, T.; Tanigawa, H.; Sakamoto, T.; Hori, A.; Muneta, I.; Kawanago, T.; Kakushima, K.; Tsutsui, K.; et al. Normally-off sputtered-MoS₂ nMISFETs with TiN top-gate electrode all defined by optical lithography for chip-level integration. *Jpn. J. Appl. Phys.* **2020**, *59* (8), 080906.